




Optical analogs of pair production and annihilation in binary waveguide arrays with a curved section

Truong X. Tran ,* Hue M. Nguyen , and Dũng C. Duong 

Department of Physics, Le Quy Don Technical University, 236 Hoang Quoc Viet str., 10000 Hanoi, Vietnam



(Received 25 November 2021; accepted 16 February 2022; published 1 March 2022)

We study theoretically and numerically the optical analogs of the relativistic quantum electron-positron dynamic pair production (PP) and annihilation processes in a single binary waveguide array (BWA) consisting of a curved section located between two straight sections at the input and output. Both of these processes can be mimicked by the breakup of beams in the curved section, which plays the role of the external oscillating field. Thanks to our scheme, we are able to observe not only the PP, but also annihilation in a single BWA with a single input beam. Moreover, this scheme allows us to obtain the numerical results for PP and annihilation probabilities by directly simulating beam propagation in binary waveguide arrays, and then compare them to the theoretical results for the same discrete model. This kind of verification demonstrates the striking excellent agreement between them in wide ranges of all relevant parameters. We also show that under certain conditions the probabilities of these two processes based on the discrete model with binary waveguide arrays agree quite well with those based on the truly continuous Dirac equation in quantum field theory.

DOI: [10.1103/PhysRevA.105.032201](https://doi.org/10.1103/PhysRevA.105.032201)

I. INTRODUCTION

A waveguide array (WA) is a remarkable system in which to explore many unusual discrete photonic effects in classical physics, such as discrete solitons [1–3], discrete diffraction [4], emission of diffractive resonant radiation [5], and so on.

Moreover, WAs have attracted a great deal of attention because they are able to provide a simple but efficient platform to study nonrelativistic quantum mechanics effects, such as Zener tunneling [6] and Bloch oscillations [3,7,8], because the system of coupled-mode equations governing light propagation processes in WAs can be converted into the Schrödinger equation. More remarkably, binary waveguide arrays (BWAs) enable us to simulate relativistic quantum mechanics effects, because under certain conditions the system of coupled-mode equations in BWAs can be converted into the Dirac equation. Thanks to that, several fundamental relativistic quantum phenomena, such as *Zitterbewegung* [9], Klein tunneling [10–12], Dirac solitons (DSs) [13], and the recently found topological Jackiw-Rebbi (JR) states [14], have been simulated both theoretically and experimentally with the help of BWAs. The JR state [15] is of primary importance in predicting the charge fractionalization phenomenon, which in its turn is fundamental in the fractional quantum Hall effect [16]. Thanks to its topological nature, the JR state in BWAs has been proved to be extraordinarily robust even when strong disturbances are applied to it [17]. This amazing feature can be used as a potential way to robustly guide photonic signals in a tightly packed network.

One extraordinary phenomenon in quantum electrodynamics (QED) rooted in the Dirac equation and first proposed by

Dirac is electron-positron pair production (PP). This process (also well known as the Schwinger mechanism [18]) is based on the quantum vacuum instability if an external electric field is applied to it [19,20]. The PP process, as interpreted by Dirac, is possible due to the existence of both negative-energy and positive-energy levels of free electrons with the energy gap $2m_e c^2$ between them [see Fig. 1(c)]. The vacuum (or Dirac sea) is filled up by these electrons located on their negative-energy levels (or states), similar to what happens with the valence band of a semiconductor. This leads to an amazing scenario in which an electron belonging to negative-energy levels in the Dirac sea can jump to positive-energy levels by absorbing an external electromagnetic (EM) field. By doing so, two particles are created: one is the electron that is now on the positive-energy levels, and the other is a hole on negative-energy levels which has just been created in the Dirac sea after the electron left the Dirac sea. This hole is the positron with a positive charge—the first ever proposed and subsequently found antimatter particle. This picture is quite similar to the more familiar generation of an electron-hole pair in semiconductors.

So far, there are two main mechanisms of PP with the participation of an EM field: the one when a *time-independent* ultrastrong electric field is applied [18], and dynamic PP when a *time-dependent* electric field is needed [21–25]. The time-independent mechanism is often interpreted as a tunneling process of a particle through a classically forbidden region, like the Klein tunneling effect [26]. This mechanism has yet to be demonstrated experimentally due to the extremely negligible PP rate with electrostatic fields available in the laboratory. Meanwhile, dynamic PP, which was first proposed in Ref. [21] with an oscillating (or time-varying) spatially homogeneous electric field, has recently attracted a great deal of attention thanks to the advent of more and more intense lasers, which can help to realize the purely laser-induced PP at the antinodes

*Corresponding author: tranxtr@gmail.com

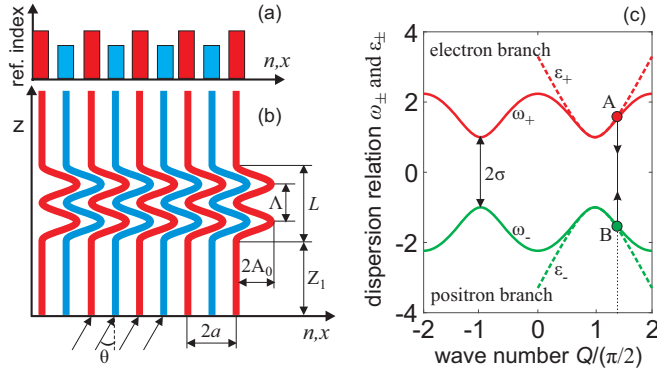


FIG. 1. (a) Scheme of a BWA made of two different types of waveguide. (b) The BWA has a curved section located between two straight sections. The curved section has the period Λ , length L , and amplitude of modulation A_0 . A beam is launched into the BWA at the angle θ . (c) Dispersion relation curves (or minibands) ω_{\pm} for BWAs and ϵ_{\pm} for the continuous model. Parameters: $\sigma = 1$ and $\kappa = 1$.

created by two laser beams propagating in opposite directions. Several other laser-based ways to observe the PP have been proposed [27,28]. However, the demonstration of the purely laser-induced PP still represents an experimental challenge.

So as with other relativistic quantum effects mentioned above, there is a strong desire to create experimentally accessible analogs of PP. Actually, several systems have been implemented for investigating matter waves, condensed matter, and optical analogs of PP [29–33]. In Ref. [30], an experimental configuration with graphene was proposed to test the Schwinger mechanism. In Ref. [31], the optical analog of the dynamic PP was investigated theoretically and numerically with a BWA consisting of a curved section at the input that is later connected to a straight section. The curved section in BWAs is needed to mimic the action of the external oscillating field in the dynamic PP. Subsequently, this idea has been experimentally realized in Ref. [33]. In these works [31,33], a Gaussian beam launched into the BWAs in the vicinity of the so-called Bragg angle represents the electrons belonging to the negative-energy state in the Dirac sea. After passing through the curved section, the Gaussian beam breaks up into two beams belonging to the positive-energy and negative-energy levels, thus the dynamic PP is mimicked via this beam breakup. However, this PP can be shown only *qualitatively* in Refs. [31,33] when the PP rate can be visually changed by varying some parameters such as the period and amplitude of the curved section. The PP rate in Refs. [31,33] cannot be verified quantitatively, because after launching a single Gaussian beam into BWAs, at least two beams with various intensity ratios (these beams belong to various energetic branches) will always occur immediately, even without the curved section. In other words, the Gaussian beam breakup always happens with or without the curved section. This makes the quantitative study of PP, which is also demonstrated through the beam breakup, quite problematic in Refs. [31,33].

To overcome the above-mentioned challenge, in this work we propose to use BWAs with a curved section not at the very beginning, but in the middle. So when a beam is launched into the system, two beams are separated distinctly in space

after splitting at the beginning. In this way, the beam breakup happening later in the curved section in the middle of BWAs is only due to the PP or annihilation. Physically speaking, it corresponds to the relevant situation in which an external field turns on and turns off again, allowing to have well-defined asymptotic states. Thanks to this, we can achieve three aims in this work: (i) first, we can unambiguously calculate the probability of the dynamic PP and annihilation through the beam propagation simulation, then compare them with the theoretical ones for verification; (ii) second, we can observe not only the PP, but also annihilation in a single BWA with a single input beam; (iii) third, we can compare the results for the PP and annihilation obtained through two models (the discrete model based on BWAs, and the continuous model in free space). As mentioned above, the PP happens when an electron jumps up from the negative-energy state into the positive-energy state as described by Dirac. Meanwhile, annihilation (or recombination) is the opposite process when an electron jumps down from the positive-energy state into the negative-energy state. In this work, the PP and annihilation probabilities obtained by direct beam simulations are demonstrated to be in striking excellent agreement with the theoretical results based on the discrete model in BWAs. We also use Dirac solitons at input instead of Gaussian beams, because DSs can overcome some shortages of a Gaussian beam when the incidence angle is close to the Bragg angle (this problem has been discussed in Ref. [12]). So, with DSs, we are able to verify the PP and annihilation probabilities in very wide ranges of parameters. Moreover, we also show that in certain parameter ranges, the results for PP and annihilation probabilities based on the discrete model agree very well with those results based on the truly Dirac continuous model in free space.

II. THEORETICAL BACKGROUND

A. Quantum-optical analogy

In this section, let us briefly focus on the theoretical background and the main theoretical results for the electron-positron PP and annihilation processes for both the discrete model with BWAs and the truly continuous Dirac model in free space. Suppose we have a BWA consisting of two different types of alternating waveguides with a curved section in the middle, as shown schematically in Figs. 1(a) and 1(b). Now we move from the fixed laboratory frame (where the array is curvy) to the waveguide reference frame (where the array appears to be straight) by using the Kramers-Henneberger transformation [34] to better analyze the light propagation process in BWAs. By doing so, light evolution in the continuous-wave regime in BWAs with Kerr nonlinearity can be described by the following dimensionless coupled-mode equations:

$$i \frac{da_n(z)}{dz} + \kappa [a_{n+1} e^{-i\Phi(z)} + a_{n-1} e^{i\Phi(z)}] - (-1)^n \sigma a_n + \gamma |a_n|^2 a_n = 0, \quad (1)$$

where a_n is the electric amplitude in the waveguide with position number n , z is the longitudinal spatial coordinate, κ and 2σ are the coupling coefficient and the propagation mismatch

between two adjacent waveguides in the arrays, respectively, and γ is the Kerr nonlinear coefficient of waveguides. In the linear regime ($\gamma = 0$), Eq. (1) are totally equivalent to Eqs. (5) in Ref. [31], whereas in a straight BWA [$\Phi(z) = 0$], Eq. (1) are exactly the same as Eqs. (1) in Ref. [13]. The phase $\Phi(z)$ in Eq. (1) takes into account the bending of the BWA axis as follows [31]:

$$\Phi(z) = \frac{2\pi n_s a \dot{x}_0(z)}{\lambda}, \quad (2)$$

where n_s is the refractive index of the BWA substrate at the excitation wavelength λ , a is the spacing between two adjacent waveguides, and $\dot{x}_0(z) = dx_0(z)/dz$ is the derivative of the axis bending profile $x_0(z)$. Suppose that Z_1 is the length of the straight section at the input of the BWA and L is the curved section length. In this work, like in Refs. [31,33], let us take a specific sinusoidal axis bending profile obeying the law $x_0(z) = -A_0 \cos[2\pi(z - Z_1)/\Lambda]$ in the interval $Z_1 \leq z \leq Z_1 + L$ with period Λ and amplitude A_0 [see Fig. 1(b)]. In this case, the dimensionless phase in the curved section is $\Phi = \Phi_0 \sin[2\pi(z - Z_1)/\Lambda]$ with

$$\Phi_0 = \frac{4\pi^2 n_s a A_0}{\lambda \Lambda}. \quad (3)$$

In straight BWAs and in the linear regime, by making the following ansatz for a plane wave:

$$a_n(Q) \sim \exp[i(Qn - \omega z)], \quad (4)$$

one can obtain the following dispersion relations for Eq. (1) [35]:

$$\omega_{\pm}(Q) = \pm \sqrt{\sigma^2 + 4\kappa^2 \cos^2 Q}, \quad (5)$$

where $Q = qa$ is the normalized dimensionless wave number of the plane wave, and q is its wave number. For the sake of brevity, Q is referred to just as a wave number later. Obviously, $Q \sim \theta$, where θ is the beam inclination angle with respect to the z -axis and represents the phase difference between adjacent waveguides.

Now let us use two assumptions: (i) the phase is small enough such that $|\Phi| \ll \pi/2$ for the whole curved section; (ii) the input beam is broad enough and excited at the input around the Bragg angle $\theta_B = \lambda/(4n_s a)$. With the first assumption we get $\exp(\pm\Phi) \simeq 1 \pm \Phi$. The second assumption lets us have the wave number around $Q_B = \pi/2$, which is necessary to convert the discrete Eq. (1) into the Dirac equation. Now one can set $\Psi_1(n) = (-1)^n a_{2n}$ and $\Psi_2(n) = i(-1)^n a_{2n-1}$, introduce the continuous transverse coordinate ξ instead of n , and the two-component spinor $\Psi(\xi, z) = (\Psi_1, \Psi_2)^T$, which satisfies the one-dimensional (1D) nonlinear Dirac equation in relativistic quantum mechanics:

$$i\partial_z \Psi = -i\kappa \hat{\sigma}_x \partial_{\xi} \Psi - 2\kappa \Phi(z) \sigma_x \Psi + \sigma \hat{\sigma}_z \Psi - \gamma G, \quad (6)$$

where $\hat{\sigma}_x$ and $\hat{\sigma}_z$ are the standard Pauli matrices, and the Kerr nonlinearity is taken into account via the last terms $G \equiv (|\Psi_1|^2 \Psi_1, |\Psi_2|^2 \Psi_2)^T$. In a straight BWA ($\Phi = 0$), Eq. (6) is exactly the same as Eq. (7) in Ref. [13]. Meanwhile, in the linear regime ($\gamma = 0$), Eq. (6) is equivalent to Eq. (7) in Ref. [31]. Note that to obtain the canonical form of the Dirac equation, one needs to introduce formal changes: $z \rightarrow t$, ξ and $n \rightarrow x$, $\kappa \rightarrow c$ (light speed), $\sigma \rightarrow mc^2/\hbar$, and

$2\Phi \rightarrow eA_x/(\hbar c)$. Now it is clear that Eq. (6) describes the evolution of an electron with mass m and charge e under the action of the external vectorial potential $\mathbf{A} = (A_x, 0, 0)$ [or the external time-varying electric field $E_x(t) = -\partial A_x(t)/\partial t$]. This external field is homogeneous in space (x or n) because the bending in BWAs is invariant in n and x [see Fig. 1(b)]. Because $z \rightarrow t$ (i.e., the longitudinal spatial coordinate z of the BWA is interpreted as time variable t), it is also clear that ω in Eq. (4) and ω_{\pm} in Eq. (5) can be interpreted as frequency (or energy).

The dispersion relations (5) are obtained for the linear discrete coupled-mode Eq. (1) in BWAs without bending. Similarly, by using the ansatz $\Psi \sim \exp[i(k\xi - \epsilon z)]$ for the linear Eq. (6) without an external field, one can obtain dispersion relations for a free relativistic electron [see Eq. (10) in Ref. [31]]:

$$\epsilon_{\pm}(k) = \pm \sqrt{\sigma^2 + \kappa^2 k^2}. \quad (7)$$

It is clear that if we write $Q = \pm\pi/2 + k/2$ and if k is small enough, then Eq. (5) is approximately reduced to Eq. (7). That is the reason why we need to launch beams around the Bragg angle (when $Q \simeq \pi/2$) to convert discrete Eq. (1) into the Dirac equation (6).

Because $z \rightarrow t$, it is also clear that ω and ϵ can be interpreted as energy (or frequency). In Fig. 1(c) we plot two branches for ω_{\pm} (solid curves for BWAs) and two branches for ϵ_{\pm} (dashed curves for the continuous model). The two upper branches ω_+ and ϵ_+ [red curves in Fig. 1(c)] are called positive-energy (or electron) branches. Meanwhile, the two lower branches ω_- and ϵ_- [green curves in Fig. 1(c)] are called negative-energy (or positron) branches. So, for the discrete model we get two minibands (ω_{\pm}), and for the continuous model we also get two minibands (ϵ_{\pm}). It is also clear in Fig. 1(c) that around the so-called Dirac point $Q \simeq \pm\pi/2$ these two models coincide with each other quite well.

B. Probability for electron-positron pair production and annihilation

The two values ω_{\pm} defined by Eq. (5) turn out to be the two eigenvalues of two corresponding Bloch modes of Eq. (1) in linear BWAs without bending [31]. One Bloch mode with ω_+ belongs to the positive-energy state, and the other with ω_- belongs to the negative-energy state. In straight BWAs ($\Phi = 0$) the transition between these two states is impossible. However, in the presence of the external oscillating electric field ($\Phi \neq 0$), this transition can be realized. By projecting an arbitrary state in a curved BWA in the linear regime (when $\gamma = 0$) onto the Bloch modes basis, one can obtain a system of equations for $r_+(z)$ and $r_-(z)$, which are the occupation amplitudes of the positive-energy and negative-energy states, respectively [31]:

$$i \frac{d}{dz} \begin{pmatrix} r_- \\ r_+ \end{pmatrix} = M(z) \begin{pmatrix} r_- \\ r_+ \end{pmatrix}, \quad (8)$$

where the 2×2 matrix $M(z)$ has the following four real components [31]:

$$M_{11}(z) = -M_{22}(z) = \frac{\sigma^2 + 4\kappa^2 \cos(Q) \cos[Q - \Phi(z)]}{\omega_+(Q)}, \quad (9)$$

$$M_{12}(z) = M_{21}(z) = \frac{2\kappa\sigma\{\cos(Q) - \cos[Q - \Phi(z)]\}}{\omega_+(Q)}. \quad (10)$$

From Eqs. (8)–(10) one can easily show that

$$i\frac{d|r_-|^2}{dz} = -i\frac{d|r_+|^2}{dz} = M_{12}(z)(r_-^*r_+ - r_-r_+^*), \quad (11)$$

thus the population $|r_+(z)|^2 + |r_-(z)|^2$ always remains constant during beams propagation. The physical meanings of $r_{\pm}(z)$ are clear: $|r_+(z)|^2$ is the probability of finding an electron (which is represented by a beam) on the positive-energy level ω_+ , whereas $|r_-(z)|^2$ is the probability of finding that electron on the negative-energy level ω_- (note that the definition of a time-dependent pair number while the external field is still turned on is a subtle issue in quantum electrodynamics [36,37]). So, the population conservation for one electron dictates that

$$|r_+(z)|^2 + |r_-(z)|^2 = 1. \quad (12)$$

It is easy to see from Eqs. (8)–(10) that in any section of BWAs where the axis is straight and parallel to the z -axis, we have $\Phi(z) = 0$, therefore $M_{12}(z) = M_{21}(z) = 0$. As a result, two quantities $|r_+(z)|^2$ and $|r_-(z)|^2$ remain constant, i.e., the transition of any electron between these two energy levels is impossible. However, in the curved section, we have $\Phi(z) \neq 0$, thus, in general, two quantities $|r_+(z)|^2$ and $|r_-(z)|^2$ change during propagation in that section, which makes the transition of electrons between the two energy levels possible. If right before entering the curved section of BWAs a beam (or electron) solely belongs to the negative-energy state ω_- in the Dirac sea, i.e., $r_-(Z_1) = 1$ [thus, $r_+(Z_1) = 0$], then the probability of the electron-positron PP at the exit of the curved section (equivalent to when the external field turns off) is $P_{pp} = |r_+(Z_1 + L)|^2$. During the beam propagation in the second (output) straight section, this value remains constant. This PP is schematically illustrated in Fig. 1(c) by the electron transition process $B \rightarrow A$ where at the end of the PP a positron (or a hole) is formed at point B , and an electron occurs at point A . From now on, we will refer to the value $P_{pp} = |r_+(Z_1 + L)|^2$ [under the initial condition $r_-(Z_1) = 1$ and $r_+(Z_1) = 0$] as the PP probability due to the total action of the external field. In Refs. [31,33], the curved section is at the very input, i.e., $Z_1 = 0$. In this case, as discussed in the Introduction and shown clearly in the next sections, any Gaussian beam always belongs to two energy levels ω_{\pm} simultaneously, thus it is very difficult to verify and measure the P_{pp} after the beam travels through the curved section. This problem is easily overcome with our scheme, as shown in the next sections.

It turns out that our scheme can also easily demonstrate the annihilation process [38,39] and verify its probability P_{an} in BWAs. If right before entering the curved section of BWAs, a beam (or electron) solely belongs to the positive-energy state ω_+ , i.e., $r_+(Z_1) = 1$ [thus, $r_-(Z_1) = 0$, and we have an electron on the positive-energy level and a positron (or a hole) on the empty negative-energy state], then the probability of annihilation or recombination of this electron-positron pair at the exit of the curved section is $P_{an} = |r_-(Z_1 + L)|^2$. During the beam propagation in the second (output) straight section, this value also remains constant. This annihilation is

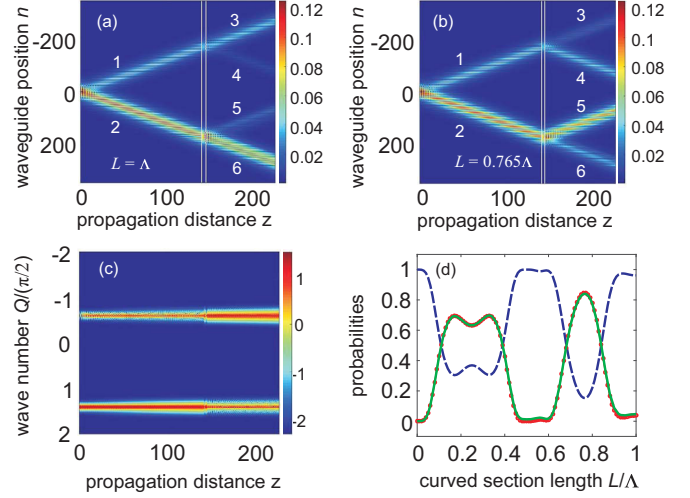


FIG. 2. (a),(b) Beams propagation in a BWA with the curved section length $L = \Lambda$ and $L = 0.765\Lambda$, respectively. (c) The evolution of the beams spectra when $L = 0.765\Lambda$. (d) The red curve with round markers represents the theoretical values for the probabilities $P_{pp} = P_{an}$. The solid green curve represents both P_{pp} and P_{an} based on beams simulations in BWAs which is in striking excellent agreement with the theoretical curve. The dashed blue curve represents the theoretical values of the probability P_s of the beam (1 or 2) staying on the same energy level after exiting the curved section. Parameters: $Q = 1.4\pi/2$, $\Lambda = 5$, $\Phi_0 = 5$, $\sigma = 1$, $\kappa = 1$, $\gamma = 1$, and $w_0 = 16$.

schematically illustrated in Fig. 1(c) by the electron transition process $A \rightarrow B$. From now on, we will refer to the value $P_{an} = |r_-(Z_1 + L)|^2$ [under the initial condition $r_+(Z_1) = 1$ and $r_-(Z_1) = 0$] as the annihilation probability due to the total action of the external field.

We want to emphasize that by solving Eqs. (8)–(10) we have obtained the same value for both P_{pp} and P_{an} under the same conditions [except for the initial ones, where we need to take $r_-(Z_1) = 1$ and $r_+(Z_1) = 0$ while computing P_{pp} , whereas $r_-(Z_1) = 0$ and $r_+(Z_1) = 1$ while computing P_{an}]. These theoretical curves for P_{pp} and P_{an} are represented by just one red curve with round markers in each of

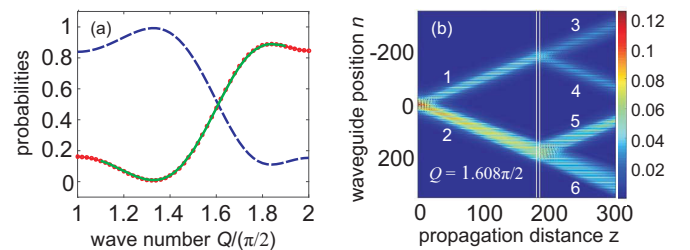


FIG. 3. (a) Dependence of probabilities on the input wave number Q : the red curve with round markers represents the theoretical values for the probabilities $P_{pp} = P_{an}$. The solid green curve represents both P_{pp} and P_{an} based on beams simulations in BWAs, which is again in striking excellent agreement with the theoretical curve. The dashed blue curve represents the theoretical values of the probability P_s . (b) Beams propagation in a BWA with the input wave number $Q = 1.608\pi/2$. Parameters: curved section length $L = \Lambda = 5$, $\Phi_0 = 5$, $\sigma = 1$, $\kappa = 1$, $\gamma = 1$, and $w_0 = 16$.

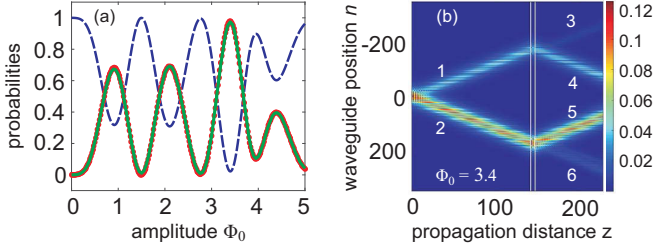


FIG. 4. (a) Dependence of probabilities on the phase amplitude Φ_0 : the red curve with round markers represents the theoretical values for the probabilities $P_{pp} = P_{an}$. The solid green curve represents both P_{pp} and P_{an} based on beams simulations in BWAs, which is again in striking excellent agreement with the theoretical curve. The dashed blue curve represents the theoretical values of the probability P_s . (b) Beams propagation in a BWA with the amplitude $\Phi_0 = 3.4$. Parameters: $L = \Lambda = 5$, $Q = 1.4\pi/2$, $\sigma = 1$, $\kappa = 1$, $\gamma = 1$, and $w_0 = 16$.

Figs. 2–6. The probabilities P_s of finding an electron on the *same* initial state (either ω_- or ω_+) after exiting the curved section, i.e., $|r_-(Z_1 + L)|^2$ [when the initial one $r_-(Z_1) = 1$] and $|r_+(Z_1 + L)|^2$ [when the initial one $r_+(Z_1) = 1$], are also exactly the same, and they are represented by just one dashed blue curve in each of Figs. 2–5. The population conservation (12) is confirmed by the fact that the dashed blue curve and the red curve with round markers in each of Figs. 2–5 are totally symmetrical to each other with respect to the horizontal axis (not shown therein) passing through the point with coordinates (0,0.5).

Equations (8)–(10) are derived from Eq. (1) for the discrete model with BWAs in the linear regime. In the same way, we can have the same Eq. (8) derived from Eq. (6) for the continuous model in the linear regime, but the components of the matrix M now read as follows [31]:

$$M_{11}(z) = -M_{22}(z) = \epsilon_+(k) - \frac{2\kappa^2 k \Phi(z)}{\epsilon_+(k)}, \quad (13)$$

$$M_{12}(z) = M_{21}(z) = -\frac{2\kappa\sigma\Phi(z)}{\epsilon_+(k)}. \quad (14)$$

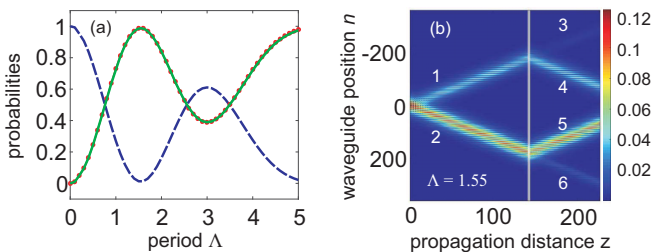


FIG. 5. (a) Dependence of probabilities on the period $\Lambda = L$ of the curved section: the red curve with round markers represents the theoretical values for the probabilities $P_{pp} = P_{an}$. The solid green curve represents both P_{pp} and P_{an} based on beams simulations in BWAs, which is again in striking excellent agreement with the theoretical curve. The dashed blue curve represents the theoretical values of the probability P_s . (b) Beams propagation in a BWA with the period $\Lambda = 1.55$. Parameters: $\Phi_0 = 3.4$, $Q = 1.4\pi/2$, $\sigma = 1$, $\kappa = 1$, $\gamma = 1$, and $w_0 = 16$.

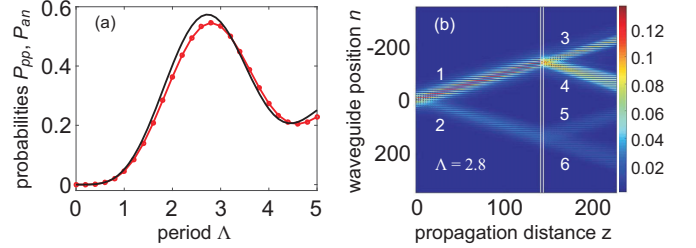


FIG. 6. (a) The probabilities P_{pp} and P_{an} as a function of the period $\Lambda = L$ of the curved section are calculated with the discrete model (the red curve with round markers) and the continuous model (solid black curve). (b) Beams propagation in a BWA with the period $\Lambda = 2.8$. Parameters: $\Phi_0 = 0.4$, $Q = 0.8\pi/2$, $L = \Lambda$, $\sigma = 1$, $\kappa = 1$, $\gamma = 1$, and $w_0 = 16$.

It is easy to prove that under two above-mentioned assumptions $|\Phi| \ll \pi/2$ and $Q \simeq \pi/2$ (or $k \simeq 0$), Eqs. (9) and (10) are reduced to Eqs. (13) and (14).

III. SIMULATIONS AND VERIFICATION OF PAIR PRODUCTION AND ANNIHILATION PROBABILITIES

In this section we systematically investigate the PP and annihilation processes by simulating the beams propagation in BWAs in the presence of a curved section. The simulations-based P_{pp} and P_{an} will be compared with their theoretical values calculated from Eqs. (8)–(10). In BWAs with Kerr nonlinearity, the analytical solution for DSs to Eq. (1) has been obtained in Ref. [13] as follows:

$$\begin{bmatrix} a_{2n}(z) \\ a_{2n-1}(z) \end{bmatrix} = \begin{bmatrix} i^{2n} \frac{2\kappa}{w_0 \sqrt{\sigma\gamma}} \operatorname{sech}\left(\frac{2n}{w_0}\right) e^{iz\left(\frac{2\kappa^2}{w_0^2\sigma} - \sigma\right)} \\ i^{2n} \frac{2\kappa^2}{w_0^2 \sigma \sqrt{\sigma\gamma}} \operatorname{sech}\left(\frac{2n-1}{w_0}\right) \tanh\left(\frac{2n-1}{w_0}\right) e^{iz\left(\frac{2\kappa^2}{w_0^2\sigma} - \sigma\right)} \end{bmatrix}, \quad (15)$$

where w_0 represents the DS width. Although the DS with solution (15) propagates along the z -axis of the BWAs, it intrinsically has two central wave numbers $Q_B = \pm\pi/2$ (see Fig. 2 in Ref. [13]) at Dirac points. Therefore, the DS can help to transform the discrete Eq. (1) into the continuous Dirac Eq. (6). The situation is completely different if a plane wave, or more often a Gaussian beam, is used. In this case, we need to launch a Gaussian beam into the BWAs in the vicinity of the Bragg angle (around the Dirac points), if we want to simulate optical analogs of relativistic quantum effects emerging from the Dirac equation [9,31,33]. This implies that a Gaussian beam

$$a_n \sim \exp\left(-\frac{n^2}{w_0^2}\right) \exp\left[i\left(\frac{\pi}{2} + \frac{k}{2}\right)n\right] \quad (16)$$

must be excited at the input of BWAs where $k \simeq 0$, and w_0 also represents the Gaussian beam width. In contrast, we need to use the initial condition for the DS as follows:

$$a_n^{\text{ini}} = a_n(0) \exp\left(in \frac{k}{2}\right), \quad (17)$$

where $a_n(0)$ in Eq. (17) is the DS taken at $z = 0$ from Eq. (15), and $k \simeq 0$. This initial condition (17) will be used below for numerically solving Eq. (1) with the help of the Runge-Kutta fourth-order method to mimic the dynamic PP and annihilation processes with a large value w_0 for broad beams to ensure that we operate in the quasilinear (low-power) regime even when the nonlinear coefficient $\gamma = 1$ is used below.

In Figs. 2(a) and 2(b) we show the beams evolution process when an initial DS with $Q = 1.4\pi/2$ (or $k = 0.4\pi$) and $w_0 = 16$ is launched into a BWA with the curved section length $L = \Lambda$ and $L = 0.765\Lambda$, respectively. The curved section [located between two vertical white lines in Figs. 2(a) and 2(b)] has the period $\Lambda = 5$. The amplitude of the phase $\Phi_0 = 5$, and the length of the first straight section is $Z_1 = 140$. As clearly shown in Figs. 2(a) and 2(b), the DS is split into two beams labeled 1 and 2 even without the curved section. This is because the initial DS is composed of two Bloch modes. As shown in Fig. 4(c) in Ref. [10], when the input angle $\theta = 1.4\theta_B$ (correspondingly, $Q = 1.4\pi/2 = 1.4Q_B$), the mode (numbered 2) belonging to the positive-energy level ω_+ will be dominantly excited, whereas the mode (numbered 1) belonging to the negative-energy level ω_- will be excited with less energy. Note also that in Fig. 4(c) in Ref. [10], four modes numbered 1–4 are excited for the model depicted in Fig. 4(a) therein, however with our tight-biding model based on Eq. (1) only two lowest modes numbered 1 and 2 with ω_{\pm} are excited. Moreover, as confirmed in Ref. [12], where all relevant parameters (except for the parameters of the external electric field) have been used in the same region, beam 2 in Figs. 2–5 demonstrates the Klein tunneling effect, so it belongs to the positive-energy state ω_+ . All beams in Figs. 2–5 in this work with label 1 (label 2) depict the beam belonging to the negative-energy state ω_- (positive-energy state ω_+). By putting the curved section in the middle of BWAs, we are able to obtain clean beams which determinedly belong solely to either ω_- or ω_+ before they go to the curved section where the dynamic PP and annihilation processes take place under action of the external field, which are shown by the beams breakup process after exciting this curved section.

As shown in Fig. 1(c) and as already pointed out in Ref. [33], “in the vicinity of the Dirac point, the two minibands have different signs in their derivative and therefore the direction of the propagating beams belonging to the two minibands is opposite.” As a result, in Figs. 2–5 all beams 1, 3, and 5 with the same propagation direction belong to the negative-energy state just like beam 1, whereas all beams 2, 4, and 6 with the same propagation direction belong to the positive-energy state just like beam 2. As shown in Figs. 2–5, beam 1 is split into two beams 3 and 4, and this is a demonstration of the dynamic PP process where the initial electron (beam 1) that is located on the negative-energy level ω_- in the Dirac sea [i.e., $r_-(Z_1) = 1$ and $r_+(Z_1) = 0$] will jump to the positive-energy level ω_+ represented by beam 4 with the PP probability $P_{pp} = I_4/I_1$, where I_m is the intensity of beam m with m runs from 1 to 6. The probability for this electron staying in the same Dirac sea on the negative-energy state ω_- represented by beam 3 is obviously equal to $1 - P_{pp} = I_3/I_1$.

On the contrary, in Figs. 2–5 beam 2 is split into two beams 5 and 6, and this is a demonstration of the annihilation process where the initial electron (beam 2) that is located on

the positive-energy level ω_+ [i.e., $r_+(Z_1) = 1$ and $r_-(Z_1) = 0$] will jump to the negative-energy level ω_- represented by beam 5 with the annihilation probability $P_{an} = I_5/I_2$. The probability for this electron staying on the same positive-energy state ω_+ represented by beam 6 is obviously equal to $1 - P_{an} = I_6/I_2$.

In Fig. 2(d) we show the dependence of various probabilities as functions of the curved section length L . The solid green curve in Fig. 2(d) (and also in Figs. 3–5) depicts the two probabilities P_{pp} and P_{an} which are obtained by the beam propagation simulations as explained above. These values are quite close to each other [for instance, $P_{pp} = 0.0408$ and $P_{an} = 0.0474$ in Fig. 2(a), whereas $P_{pp} = 0.8423$ and $P_{an} = 0.8396$ in Fig. 2(b)], so we just use the green curve for both P_{pp} and P_{an} in Figs. 2–5 (otherwise, all three curves will be on top of each other, which will make it difficult to see each of them clearly). As clearly shown in Figs. 2–5, the theoretical (red curve with round markers) and simulations-based values for P_{pp} and P_{an} are in striking excellent agreement.

In Fig. 2(c) we demonstrate the evolution in the (Q, z) -plane of the spectra of beams shown in Fig. 2(b). This can be done by getting the Fourier transform for a_n at each distance z . Each beam in Fig. 2(c) has two spectral components around the input wave number $Q = 1.4\pi/2$ and around $Q' = -0.6\pi/2$. The spacing between Q and Q' is exactly equal to π , i.e., the period of the Brillouin zones shown in Fig. 1(c) for the discrete model. This feature is also true even for a DS consisting of just one beam parallel to the z -axis during propagation (when at input $k = 0$, thus input wave number $Q = \pi/2$) as shown in Fig. 2 in Ref. [13]. Figure 2(c) confirms that each of the dynamical PP and annihilation processes in BWAs just happens with one wave number Q .

In Fig. 3(a) we show the dependence of various probabilities on the input wave number Q while fixing all other parameters such as the curved section length $L = \Lambda = 5$ and the phase amplitude $\Phi_0 = 5$. Figure 3(a) shows that the theoretical curve (the red one with round markers) for $P_{pp} = P_{an}$ and the corresponding simulations-based curve (solid green curve) are again in striking excellent agreement. Note that in Fig. 3(a) we just plot the simulations-based curve (solid green one) in the interval $Q \in [1.1\pi/2; 1.9\pi/2]$ because by getting closer to Dirac point $Q = \pi/2$ and point $Q = \pi$ all beams 1–6 become closer to each other in space (when $Q = \pi/2$ all beams 1–6 become one single beam parallel to the z -axis (see Fig. 2 in Ref. [13]), thus it is difficult to observe the beam breakup process. For input Gaussian beams, it is even more difficult to form separated collimated beams with $Q \simeq \pi/2$ or π as already shown in Ref. [12]. As an example, in Fig. 3(b) we show the beam propagation simulation when $Q = 1.608\pi/2$, where the probabilities $P_{pp} = P_{an} = 0.5$. This is clearly proved in Fig. 3(b) where due to the dynamic PP beam 1 is split into two beams (3 and 4) with equal intensity, and the annihilation process makes beam 2 split into two beams (5 and 6) with equal intensity as well.

In Fig. 4(a) we show the dependence of various probabilities on the phase amplitude Φ_0 while fixing all other parameters such as the curved section length $L = \Lambda = 5$ and the input wave number $Q = 1.4\pi/2$. Figure 4(a) shows that the theoretical curve (the red one with round markers)

for $P_{pp} = P_{an}$ and the corresponding simulations-based curve (solid green curve) are also in perfect agreement. As an example, in Fig. 4(b) we show the beam propagation when $\Phi_0 = 3.4$ and the probabilities $P_{pp} = P_{an} = 0.97$, where 97% of energy from beam 1 is transferred to beam 4 due to the dynamic PP, and 97% of energy from beam 2 is transferred to beam 5 due to the annihilation process.

In Fig. 5(a) we show the dependence of various probabilities on the period Λ which is also set to be the length L of the curved section while fixing all other parameters such as the phase amplitude $\Phi_0 = 3.455$ and the input wave number $Q = 1.4\pi/2$. Figure 5(a) confirms again the perfect agreement between the theoretical curve and the simulations-based curve for $P_{pp} = P_{an}$. As an example, in Fig. 5(b) we show the beam propagation when $\Lambda = 1.55$. As a result, the probabilities $P_{pp} = P_{an} = 0.99$, where 99% of energy from beam 1 is transferred to beam 4 due to the dynamic PP, and 99% of energy from beam 2 is transferred to beam 5 due to the annihilation process.

In this section, we have shown that the results for P_{pp} and P_{an} based on simulating the DSs propagation governed by nonlinear (i.e., $\gamma = 1$) Eq. (1) are in perfect agreement with the theoretical results for P_{pp} and P_{an} based on Eqs. (8)–(10) [which are derived from linear Eq. (1) with $\gamma = 0$] in wide ranges of all relevant parameters. We just need to make sure that the peak input intensity of DSs is small enough (simply by choosing a large beam width parameter w_0 for DSs) to guarantee that we operate in the quasilinear (low-power) regime. The influence of nonlinearity when intense DSs are used will be investigated elsewhere.

IV. COMPARISON BETWEEN THE DISCRETE AND CONTINUOUS MODELS

In this section, we compare the theoretical results for the probabilities P_{pp} and P_{an} based on the discrete model [Eqs. (8)–(10)] with those based on the continuous model of the Dirac equation [i.e., Eqs. (8), (13), and (14)]. As mentioned in Sec. II, these results should agree quite well with each other when two conditions hold true: (i) we operate around Dirac points ($Q \simeq \pi/2$); (ii) phase Φ is small enough ($|\Phi| \ll \pi/2$). Indeed, as an example, in Fig. 6(a) we fix the

phase amplitude $\Phi_0 = 0.4$ and the input wave number $Q = 0.8\pi/2$ while plotting P_{pp} and P_{an} as a function of the period Λ (which is also set to be equal to the length $L = \Lambda$) of the curved section, where the red curve with round markers is based on the discrete model and the solid black curve is based on the continuous model. At $\Lambda = 2.8$, the discrete model in Fig. 6(a) reaches its maximum $P_{pp} = P_{an} \simeq 0.55$, which is again in perfect agreement with the simulation-based result for Eq. (1) (also $\simeq 0.55$) shown in Fig. 6(b). On the other hand, when $\Lambda = 2.8$, the continuous model gives the result $P_{pp} = P_{an} \simeq 0.57$.

Note that in Fig. 6 we use the input wave number $Q = 0.8\pi/2 < Q_B = \pi/2$, whereas in Figs. 2–5 we use the input wave number $Q > Q_B = \pi/2$. By checking the Klein tunneling effect (not shown here) for beams 1 and 2 in Fig. 6, it turns out that this effect only happens with beam 1 but not with beam 2, so now beam 1 belongs to the positive-energy state ω_+ , and the breakup of beam 1 into beams 3 and 4 in Fig. 6 simulates the annihilation process. Meanwhile, beam 2 belongs to the negative-energy state ω_- , and the breakup of beam 2 into beams 5 and 6 in Fig. 6 simulates the dynamic PP process.

V. CONCLUSIONS

In conclusion, we have theoretically and numerically demonstrated the optical analogs of electron-positron dynamic PP and annihilation in BWAs with a curved section located in the middle to mimic the external oscillating electric field. This system allows us to simultaneously observe the two processes and determine unambiguously their probabilities by beams propagation simulations in BWAs, which are shown to be in perfect agreement with the theoretical results. Under some specified conditions, the probabilities based on this discrete model agree well with those based on the continuous Dirac equation. Our findings show that BWAs are an amazing photonic system to mimic fundamental quantum relativistic phenomena in QED.

ACKNOWLEDGMENTS

This work was funded by Vingroup and supported by Vingroup Innovation Foundation (VINIF) under project code VINIF.2021.DA00001.

-
- [1] D. N. Christodoulides and R. I. Joseph, *Opt. Lett.* **13**, 794 (1988).
 - [2] Y. S. Kivshar and G. P. Agrawal, *Optical Solitons: From Fiber to Photonic Crystals*, 5th ed. (Academic, New York, 2003).
 - [3] D. N. Christodoulides, F. Lederer, and Y. Silberberg, *Nature (London)* **424**, 817 (2003).
 - [4] A. L. Jones, *J. Opt. Soc. Am.* **55**, 261 (1965).
 - [5] T. X. Tran and F. Biancalana, *Phys. Rev. Lett.* **110**, 113903 (2013).
 - [6] M. Ghulinyan, C. J. Oton, Z. Gaburro, L. Pavesi, C. Toninelli, and D. S. Wiersma, *Phys. Rev. Lett.* **94**, 127401 (2005).
 - [7] T. Pertsch, P. Dannberg, W. Elflein, A. Bräuer, and F. Lederer, *Phys. Rev. Lett.* **83**, 4752 (1999).
 - [8] G. Lenz, I. Talanina, and C. M. de Sterke, *Phys. Rev. Lett.* **83**, 963 (1999).
 - [9] F. Dreisow, M. Heinrich, R. Keil, A. Tünnermann, S. Nolte, S. Longhi, and A. Szameit, *Phys. Rev. Lett.* **105**, 143902 (2010).
 - [10] S. Longhi, *Phys. Rev. B* **81**, 075102 (2010).
 - [11] F. Dreisow, R. Keil, A. Tünnermann, S. Nolte, S. Longhi, and A. Szameit, *Europhys. Lett.* **97**, 10008 (2012).
 - [12] Q. Nguyen-The and T. X. Tran, *J. Opt. Soc. Am. B* **37**, 1911 (2020).
 - [13] T. X. Tran, S. Longhi, and F. Biancalana, *Ann. Phys.* **340**, 179 (2014).
 - [14] T. X. Tran and F. Biancalana, *Phys. Rev. A* **96**, 013831 (2017).
 - [15] R. Jackiw and C. Rebbi, *Phys. Rev. D* **13**, 3398 (1976).

- [16] R. B. Laughlin, *Rev. Mod. Phys.* **71**, 863 (1999).
- [17] T. X. Tran, *J. Opt. Soc. Am. B* **36**, 2559 (2019).
- [18] J. Schwinger, *Phys. Rev.* **82**, 664 (1951).
- [19] E. S. Fradkin, D. M. Gitman, and S. M. Schvartsman, *Quantum Electrodynamics with Unstable Vacuum* (Springer, Berlin, 1991).
- [20] H. K. Avetissian, *Relativistic Nonlinear Electrodynamics* (Springer, New York, 2006).
- [21] E. Brezin and C. Itzykson, *Phys. Rev. D* **2**, 1191 (1970).
- [22] V. S. Popov, *JETP Lett.* **18**, 255 (1973).
- [23] H. K. Avetissian, A. K. Avetissian, G. F. Mkrtchian, and K. V. Sedrakian, *Phys. Rev. E* **66**, 016502 (2002).
- [24] M. Ruf, G. R. Mocken, C. Muller, K. Z. Hatsagortsyan, and C. H. Keitel, *Phys. Rev. Lett.* **102**, 080402 (2009).
- [25] F. Gelis and N. Tanji, *Prog. Part. Nucl. Phys.* **87**, 1 (2016).
- [26] F. Sauter, *Z. Phys.* **69**, 742 (1931).
- [27] S. S. Bulanov, V. D. Mur, N. B. Narozhny, J. Nees, and V. S. Popov, *Phys. Rev. Lett.* **104**, 220404 (2010).
- [28] A. Gonoskov, I. Gonoskov, C. Harvey, A. Ilderton, A. Kim, M. Marklund, G. Mourou, and A. Sergeev, *Phys. Rev. Lett.* **111**, 060404 (2013).
- [29] R. Schützhold, *Adv. Sci. Lett.* **2**, 121 (2009).
- [30] D. Allor, T. D. Cohen, and D. A. McGady, *Phys. Rev. D* **78**, 096009 (2008).
- [31] S. Longhi, *Phys. Rev. A* **81**, 022118 (2010).
- [32] N. Szpak and R. Schützhold, *Phys. Rev. A* **84**, 050101(R) (2011).
- [33] F. Dreisow, S. Longhi, S. Nolte, A. Tünnermann, and A. Szameit, *Phys. Rev. Lett.* **109**, 110401 (2012).
- [34] S. Longhi, *Laser Photon. Rev.* **3**, 243 (2009).
- [35] A. A. Sukhorukov and Y. S. Kivshar, *Opt. Lett.* **27**, 2112 (2002).
- [36] R. Dabrowski and G. V. Dunne, *Phys. Rev. D* **94**, 065005 (2016).
- [37] A. Ilderton, *Phys. Rev. D* **105**, 016021 (2022).
- [38] C. C. Gerry, Q. Su, and R. Grobe, *Phys. Rev. A* **74**, 044103 (2006).
- [39] Y. Nishida, *Phys. Rev. D* **104**, L031902 (2021).